Dynamical crossover at the liquid-liquid transformation of a compressed molten alkalI metal

Bryk, Taras ; De Panfilis, Simone ; Gorelli, Federico A ; Gregoryanz, Eugene ; Krisch, Michael ; Ruocco, Giancarlo ; Santoro, Mario ; Scopigno, Tullio ; Seitsonen, Ari P

Abstract: Density-driven phase transformations are a known phenomenon in liquids. Pressure-driven transitions from an open low-density to a higher-density close-packed structure were observed for a number of systems. Here, we show a less intuitive, inverse behavior. We investigated the electronic, atomic, and dynamic structures of liquid Rb along an isothermal line at 573 K, at 1.2-27.4 GPa, by means of ab initio molecular dynamics simulations and inelastic x-ray scattering experiments. The excellent agreement of the simulations with experimental data performed up to 6.6 GPa validates the overall approach. Above 12.5 GPa, the breakdown of the nearly-free-electron model drives a transition of the pure liquid metal towards a less metallic, denser liquid, whose first coordination shell is less compact. Our study unveils the interplay between electronic, structural, and dynamic degrees of freedom along this liquid-liquid phase transition. In view of its electronic nature, we believe that this behavior is general for the first group elements, thus shedding new light into the high-pressure properties of alkali metals.

DOI: https://doi.org/10.1103/PhysRevLett.111.077801

Dynamical crossover at the liquid-liquid transformation of a compressed molten alkali metal.

Taras Bryk,[1,2] Simone De Panfilis,[3,1] Federico A Gorelli,[4,5] Eugene Gregoryanz,[6] Michael Krisch,[7] Giancarlo Ruocco,[1,5] Mario Santoro,[8] Tullio Scopigno,[1,5] and Ari P Seitsonen[9]

[1]*Dipartimento di Fisica, Università di Roma "Sapienza", I-00185, Roma, Italy*

[2]*Institute for Condensed Matter Physics of NASU, UA-79011 Lviv, Ukraine*

[3]*Centre for Life Nano Science IIT@Sapienza,*
Istituto Italiano di Tecnologia, I-00161, Roma, Italy

[4]*European Laboratory for Non Linear Spectroscopy,*
I-50019 Sesto Fiorentino, Firenze, Italy

[5]*IPCF-CNR, c/o Università di Roma "Sapienza", I-00185, Roma, Italy*

[6]*Centre for Science at Extreme Conditions and School of Physics and Astronomy,*
University of Edinburgh, Edinburgh, EH9 3JZ, United Kingdom

[7]*European Synchrotron Research Facility, F-38043 Grenoble, France*

[8]*IFAC-CNR, I-50019 Sesto Fiorentino, Italy*

[9]*Institute for Physical Chemistry, University of Zürich, CH-8057 Zürich, Switzerland*

(Dated: July 27, 2013)

Abstract

Density driven phase transformations are a known phenomenon in liquids. Pressure driven transitions from an open low density to a higher density close packed structure were observed for a number of systems. Here we show a less intuitive, inverse behaviour. We investigated the electronic and atomic structures of liquid Rb along an isothermal line at 573 K, at $1.2-27.4$ GPa, by means of ab initio molecular dynamics simulations and inelastic x-ray scattering experiments. The excellent agreement of the simulations with experimental data performed up to 6.6 GPa validates the overall approach. Above 12.5 GPa the breakdown of the nearly-free electron model drives a transition of the pure liquid metal towards a less metallic, denser liquid, whose first coordination shell is less compact. Our study unveils the interplay between electronic, structural and dynamic degrees of freedom along this liquid-liquid phase transition. In view of its electronic nature, we believe that this behavior is general for the first group elements, thus shedding new light into the high pressure properties of alkali metals.

PACS numbers: 61.25.Mv, 61.20.Ja, 61.20.Lc

Keywords: liquid metals, structural transformations, high pressure, ab initio molecular dynamics, inelastic x-ray scattering

The high-pressure behavior of solids and liquids is one of the most fascinating topics in modern condensed matter physics. Especially in crystalline metals, the extreme conditions can lead to several structural transformations, appearance of exotic structures, and unusual pressure-induced metal-nonmetal transitions [1–7]. The case of liquid metals under high pressure is much less investigated: only a few studies suggested structural transformations affecting the short-range order, resembling those reported in solids. Recently, a possible metal-nonmetal transition in liquid Na [8] and a tetrahedral clustering of nearest neighbors in liquid Li at pressure $\sim$ 150 GPa [9] were reported using *ab initio* molecular dynamics (AIMD) simulations. Jointly with experimental observations in solid Li [10] these discoveries set a stage of unusual properties and new structural transformations in liquid metals at high pressures and temperatures. AIMD simulations were also successfully applied in high-pressure studies of structural features of other liquid alkali metals, such as Cs [11, 12] and Rb [13], and in liquid Si [14].

The opinion that alkali metals are, due to their nearly-free-electron character, prototypical simple liquids has always been a well buttressed one. Recent discoveries, however, indicate that this paradigm no longer holds at extreme conditions. Remarkably, high pressure dynamical properties – such as single particle diffusion and sound propagation – are largely unexplored for liquid alkali metals [15]. Yet, the knowledge of the dynamics has strong implications on the physical state of a system. We have recently shown that the collective dynamics changes dramatically with pressure, allowing one to identify liquid-like and gas-like behaviour even beyond the critical point [16, 17].

Among the alkali metals, Rb possesses the least known phase diagram [18]. Solid Rb is experimentally known to exist in six structural phases [2] up to $\sim$ 30 GPa [19], including the exotic Rb-III [20] and Rb-IV phases [21, 22]. The latter has an incommensurate composite structure, comprised of a tetragonal host framework and a simple body-centered tetragonal guest [21, 22]. The melting curve is known only up to $\sim$ 10 GPa, and the structure of liquid Rb at pressures higher than 6.1 GPa is completely unknown. Here, we present a combined AIMD and experimental study of liquid Rb above the melting line, shedding new light onto the structural and dynamic features under high pressure. The computational effort was initiated by inelastic x-ray scattering (IXS) experiments on liquid Rb, performed for pressures up to 6.6 GPa at 573 K, and were extended for much higher pressures because of the observed increase of the calculated ratio of specific heats γ, while for ordinary liquids

γ is expected to decrease with pressure.

AIMD simulations were performed at 8 different densities and $T = 573$ K in liquid Rb using a system of 300 particles in a cubic box. The initial configurations were taken from classical molecular dynamics simulations with subsequent equilibration over ~ 5 ps in the NVT ensemble. Production runs took at least 38 ps at each pressure. The electron-ion interactions for Rb were represented by Projector-Augmented-Wave (PAW) potentials [23] with 7 valence electrons in order to take into account semi-core electrons. The electron subsystem was treated within the density functional theory with the generalized gradient approximation in the Perdew-Burke-Ernzerhof formulation [24, 25] applied for the exchange-correlation functional. The cut-off energy in the expansion of electron wave functions in a plane wave basis was 290 eV. For the construction of the electron density only the Γ point of the Brillouin zone was used; this was sufficient in our large simulated system [26] and according to previous tests in other alkali metals [8, 9]. The smallest wave numbers k sampled in our *ab initio* simulations ranged from 0.224Å^{-1} at pressure 1.2 GPa to 0.322Å^{-1} at P=27.4 GPa.

The dynamic properties were calculated from the time evolution of the particles' positions, velocities and forces. The diffusion constant was obtained from the Kubo integrals of the velocity autocorrelation functions and was in excellent agreement with the values of the diffusivity D calculated from the linear long-time asymptotes of the mean square displacements. The collective dynamics was studied by means of the density-density and longitudinal current-current time correlation functions. The length of the time correlation functions was taken to be 12 ps in order to calculate the fine resolution of the current spectral functions $C^L(k,\omega)$, where ω is the frequency. The peak positions of $C^L(k,\omega)$ resulted in the dispersion of collective excitations, and the corresponding values of the apparent speed of sound (c_{app}) were estimated at the smallest wave numbers. For analysis of the time correlation functions and estimation of the adiabatic speed of sound c_s and the ratio of specific heats γ we used the approach of Generalized Collective Modes (GCM) [27] based on generalized hydrodynamics and well-elaborated thermo-viscoelastic dynamic model [28, 29].

For the purpose of our work, the electron localization function (ELF), which measures the probability of finding an electron in a specific portion of space relative to a reference electron, was directly derived by the electron density calculated by the AIMD simulations through the DFT formalism [30].

The IXS experiment was performed at the ID28 beamline of the ESRF. High purity Rb (99.6% purity from Sigma Aldrich) was loaded in a membrane driven DAC equipped with 600 μm culet size diamond anvils. The sample was placed in a 150 μm diameter and 80 μm thick hole in a pre-indented Re gasket. The DAC was placed inside a vacuum chamber especially designed for IXS experiments on fluids [31]. The dynamic structure factor was simultaneously measured at nine different momentum transfer values in the range $2 - 15$ nm^{-1}. The overall instrument resolution was set at 1.4 meV using the (12 12 12) Si reflection of the analyzers ($E = 23.725$ keV). Three experimental points were measured along an isotherm at 573 K up to 6.6 GPa. The pressure was estimated by means of the Re gasket diffraction lines with an uncertainty of about 0.5 GPa. The sample quality was checked several times by measuring the static structure factor $S(Q)$ and comparing it to literature data [32].

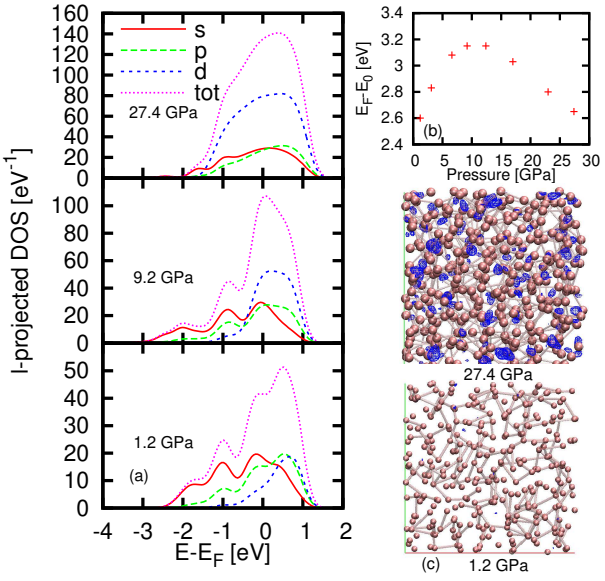

FIG. 1: Pressure dependence of the electronic density of states. Pressure dependence of the l-projected electronic states (a) and of the width of the conduction band (b). E_0 and E_F are the bottom of the conduction band and Fermi energy, respectively. (c) The isosurface (online: blue color) of ELF at the value 0.60 in snapshots of simulations at pressures 27.4 and 1.2 GPa.

The electronic density of states measured by the AIMD computational experiments displays remarkable changes as a function of pressure (see Fig.1.a.) The location of the Fermi level in the conduction band provides evidence of metallic behavior throughout the explored thermodynamic region. In stark contrast to liquid Li at very high pressures [9], we do not

observe the appearance of any pseudogap in the electronic density of states at the Fermi level. In simple metals the nearly free electron model predicts an increase of the Fermi energy with pressure, due to the broadening of the conduction band. Accordingly, E_F monotonically shifts towards higher energies with respect to the bottom of the conduction band. This is not what we observe in liquid Rb at high pressures. The distance from the Fermi energy to the bottom of conduction band, $E_F - E_0$, increases up to $\sim 12 - 13$ GPa as in simple metals, but it decreases afterwards (Fig.1.b). Figure 1 suggests that the non-simple metallic behavior of $E_F - E_0$ versus pressure is due to the increased filling of the $4d$-electron band: the conduction electrons that are mainly of s-type at pressure ~ 1.2 GPa, acquire a predominantly d-type character at high pressures.

In Fig.1.c we show the ELF isosurfaces calculated for the lowest and highest pressures investigated in our simulations. They give an insight into the spatial distribution of the electron wave functions at the two pressures. As expected, only a few regions reach an ELF reference value of 0.60 at P=1.2 GPa, while at 27.4 GPa the electrons are strongly localized in the interstitial regions, reaching ELF values as high as 0.91. Yet, in contrast to solid systems [33] where the voids in interstitial regions can be well separated and a gap appears at the Fermi level, in the case of liquid Rb the interstitial regions are interconnected. This provides the rationale for our explanation of the metallic nature of liquid Rb at high pressure.

The observed electronic behaviour is mirrored in its structural and dynamical counterparts. The pair correlation function $g(R)$ calculated for different pressures is shown in Fig.2.a. The main peak of $g(R)$ increases in height, gets narrower and shifts towards smaller R upon compression. The shift of its position, R_{max}, as a function of the atomic volume V is shown in Fig.2.c and shows a reduction of the mean distance between nearest neighbors from 4.42 Å at 1.2 GPa to 3.04 Å at 27.4 GPa. In agreement with simulations of liquid Cs at high pressures [12], this dependence is a monotonic function of pressure, although for P higher than 12.4 GPa a substantial deviation from the linear behavior predicted by the uniform compression model [32] is observed. The evolution of the number of next-nearest neighbors (NNN), i.e. the mean number of particles in the first coordination shell, shows a remarkable behavior versus pressure (see Fig.2.b). Below 10 GPa NNN stays constant at ~ 13.5 particles. Above 12.4 GPa we observe a gradual reduction of the number of particles in the first coordination shell, with NNN reaching ~ 10.4 at 27.4 GPa. This is consistent

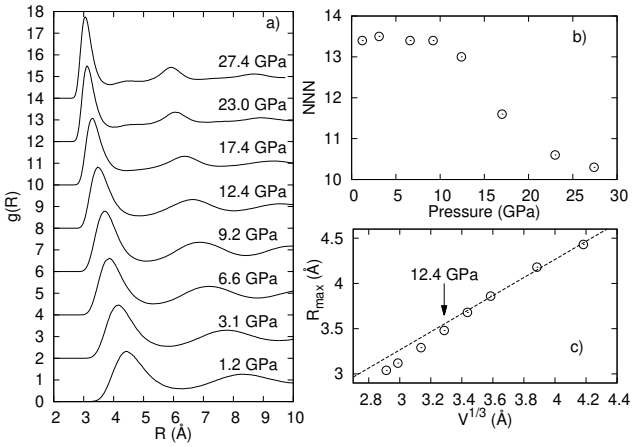

FIG. 2: Pressure dependence of atomistic structure. (a) Evolution of the pair distribution functions $g(R)$ in liquid Rb at 573 K in the pressure range 1.2-27.4 GPa (curves are vertically shifted by 2 for clarity). (b) Number of nearest neighbours as a function of pressure. (c) Position of the main peak of the $g(R)$ (symbols) versus $V^{1/3}$ and the prediction of the uniform compression model (dashed line). The arrow indicates the pressure at which R_{max} deviates by the uniform compression behavior. It is consistent with the pressure at which the number of nearest neighbours starts to deviate from an average value of 13.5.

with the appearance of a secondary maximum around 4-5 Å developing between 12.4 GPa and 27.4 GPa, strongly suggestive of a second coordination shell. Remarkably, the bcc-fcc-liquid Rb triple point is roughly located in the P-T region 0.93-10.2 GPa and 490-520 K [18], and above 12 GPa solid Rb undergoes a further phase transition to Rb-III associated with a large volume change [19]. The structural transformation that we observe occurs in the proximity of this portion of the solid phase diagram, at striking similarity with liquid Cs under pressure [12], where an analogous reduction of the NNN from 13 to 7-8 was observed at 493 K, in the pressure region of the bcc-to-fcc transition. We remark that the observed structural deviation from a simple liquid behavior in Rb at high pressure coincides with the non monotonic trend of its electronic counterpart, i.e. the structural changes are supported by the transformations occurring in the electronic states.

The analysis of thermodynamic properties provides further support to the existence of a liquid-liquid phase transition. While we could estimate the specific heat at constant volume c_V, the one at constant pressure c_P cannot be directly obtained from AIMD simulations. On the contrary, the ratio $\gamma = c_P/c_V$ can be determined within the GCM scheme by the

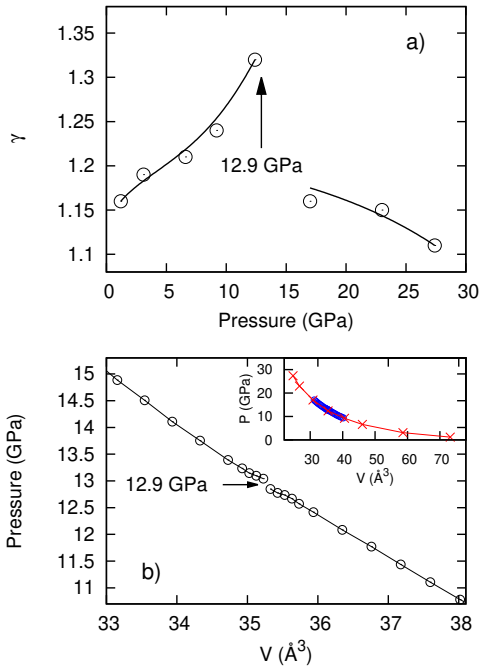

FIG. 3: Thermodynamic properties of liquid Rb at 573 K, as a function of pressure. (a) The ratio of the specific heats, γ, versus pressure. Lines are guides for the eye. (b) P-V equation of state of liquid Rb at 573 K. The reduction of the P-V slope in the region about 12.9 GPa (arrow) corresponds to an increasing isothermal compressibility. In the inset, the full P-V curve is shown: results obtained from AIMD simulations with 300 (cross symbols) and 64 (plus symbols) particles.

generalized hydrodynamic analysis of the density-density time correlation functions. The pressure dependence of γ is shown in Fig.3.a. It shows a steep increase in the low pressure region up to about 13 GPa, followed by reduced γ values above 15 GPa. This testifies the existence of a Widom line between a low-density and high-density phase, as suggested for the case of supercooled water [34]. A direct inspection of the P-V equation of state (Fig.3) corroborates our conclusions. Specifically, a finer inspection of the region $9-17$ GPa, using a reduced system containing 64 Rb atoms shows a slope discontinuity for V$\simeq 35.0-35.5$ Å^3. This implies a rapid increase in the isothermal compressibility $\kappa_T = -V^{-1}(\partial V/\partial P)_T$ at the pressures ~ 13 GPa, again a clear signature of a liquid-liquid transition occurring in compressed liquid Rb.

The liquid-liquid transition is revealed also by looking at the dynamic properties of liquid Rb at high pressure. It is well documented that the adiabatic sound velocity reflects the combined critical behavior of structure and thermodynamics, namely $\gamma/S(k \to 0)$, being

$S(k)$ the static structure factor [35]. Furthermore, according to the theory of dynamic critical phenomena [36, 37], it is possible to observe a reduction in the adiabatic speed of sound by approaching the liquid-gas transition or the demixing limit in binary liquids. Remarkably, we show in Fig.4 a slope discontinuity in the pressure behavior of the instantaneous, hypersonic sound velocity as determined by GCM applied to the AIMD data, which can not be simply traced back to the above mentioned structural and thermodynamical criticalities. Such anomalous behavior of a collective, non adiabatic dynamical property pairs with the single particle dynamics counterpart, as emphasized by the pressure dependence of Rb atoms diffusivity, D, shown in Fig.4. At $\sim 10-13$ GPa $D(P)$ flattens, providing an evidence of an essential reduction in the core radius of Rb atoms [38].

To validate the goodness of the computational approach, we benchmarked the dynamic structure properties obtained by the AIMD simulations against IXS experimental data (red points in Fig. 4) up to 6.6 GPa. The agreement on the sound velocity is excellent but not exclusive, as the overall similarity extends over the entire $S(k,\omega)$ functions.

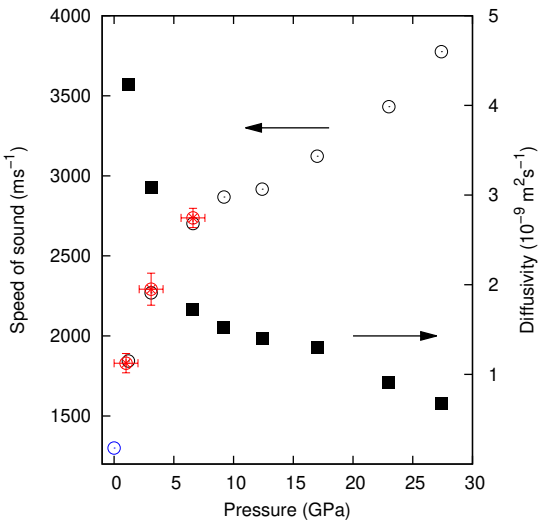

FIG. 4: Pressure dependence of dynamic properties. The diffusion coefficient D (filled symbols), and the apparent speed of sound $c_{\rm app}$ (open symbols) in liquid Rb at 573 K as a function of pressure. Red dots are experimental findings after IXS measurements. The ambient pressure point (blue symbol) measured at 600 K by INS is from ref. [39].

Liquid polyamorphism [40] in alkali metals and other systems showing melting curve maxima was predicted within the Rapoport 2-state model [41]. It was noted, there, that the regular solution model used to fit the data implied the possible existence of a first-order

liquid-liquid phase transition at some low T, below the stable liquidus, terminating in a critical point hidden in the undercooled liquid, and inferring a Widom line crossing in the equilibrium liquid. The results of our study are very much in agreement with the suggestions of the 2-state model, and we believe this further confirms our conclusions of a liquid-liquid transformation in liquid Rb at high pressure.

In summary, exploring the pressure range $1.2 - 27.4$ GPa along an isotherm by a combination of AIMD and IXS experiments, we witness the breakdown of the nearly free electron model in liquid Rubidium, providing convincing evidence of a liquid-liquid phase transition. This phenomenon can be traced back to an enhancement of the electronic localization, from a simple low-density metallic liquid to an essentially $4d$-electron high-density liquid. The $4d$ band becomes occupied at high pressures and the valence electrons have predominantly d-character, thus favoring covalent bonding. Accordingly, structural and thermodynamic properties show the typical features associated with a phase transition. Most interesting, we unraveled the critical behaviour of collective and single particle dynamics, i.e. a sharp change of slope occurring upon compression at the transition, suggestive of Widom line crossing, recently proposed for the case of water [34] and supercritical fluids [16, 17].

The supercomputer allocation time within the CINECA project "Dynamics and thermodynamics of compressed liquid metals studied with ab-initio molecular dynamics" is gratefully acknowledged. The calculations have been performed using the ab-initio total-energy and molecular dynamics program VASP (Vienna ab-initio simulation program) developed at the Institute für Materialphysik of the Universität Wien [42, 43]. We acknowlwdge the helpful technical assitance of the ESRF staff during the IXS experimental campaign. T.S. has received funding from the European Research Council under the European Communitys Seventh Framework Program (FP7/20072013)/ERC grant Agreement FEMTOSCOPY No. 207916.

[1] M. Hanfland, K. Syassen, N.E. Christensen and D.L. Novikov *Nature* **408**, 174 (2000).

[2] G.J. Ackland and I.R. Macleod *New J. Phys.* **6**, 138 (2004).

[3] E. Gregoryanz, L.F. Lundegaard, M.I. McMahon, C.L. Guillaume, R.J. Nelmes and M. Mezouar *Science* **320** 1054 (2008)..

[4] Y. Ma, M. Eremets, A.R. Oganov, Y. Xie, I. Trojan, S. Medvedev, A.O. Lyakhov, M. Valle and V. Prakapenka *Nature* **458**, 182 (2008).

[5] C.L. Guillaume, E. Gregoryanz, O. Degtyareva, M.I. McMahon, M. Hanfland, S. Evans, M. Guthrie, S.V. Sinogeikin and H.-K. Mao *Nature Phys.* **7**, 211 (2011).

[6] M. Marques, M. Santoro, C.L. Guillaume, F.A. Gorelli, J. Contreras-Garcia, R.T. Howie, A.F. Goncharov and E. Gregoryanz *Phys. Rev. B* **83**, 184106 (2011).

[7] F.A. Gorelli, S.F. Elatresh, C.L. Guillaume, M. Marques, G.J. Ackland, M. Santoro, S.A. Bonev, E. Gregoryanz *Phys Rev Lett* **108**, 055501 (2012).

[8] J.-Y. Raty, E. Schwegler, S.A. Bonev *Nature* **449**, 448-451 (2007).

[9] I. Tamblyn, J.-Y. Raty, S.A. Bonev *Phys Rev Lett* **101**, 075703 (2008).

[10] T. Matsuoka, K. Shimizu *Nature* **458**, 186-189 (2008).

[11] S. Falconi, L.F. Lundegaard, C. Hejny, M.I. McMahon *Phys Rev Lett* **94**, 125507 (2005).

[12] S. Falconi, G.J. Ackland *Phys Rev B* **73**, 184204 (2006).

[13] F. Shimojo, Y. Zempo, K. Hoshino, M. Watabe *Phys Rev B* **55**, 5708-5711 (1997).

[14] P.Ganesh and M. Widom, *Phys. Rev. Lett.* **102**, 075701 (2009).

[15] V. Giordano, G. Monaco *J Chem Phys* **131**, 014501 (2009).

[16] G.G. Simeoni, T. Bryk, F.A. Gorelli, M. Krisch, G. Ruocco, M. Santoro, T. Scopigno *Nature Phys* **6**, 503-507 (2010).

[17] F.A. Gorelli, T. Bryk, M. Krisch, G. Ruocco, M. Santoro, T. Scopigno *Sci Rep* **3**, 1203 (2013).

[18] R. Boehler, C.-S. Zha *Physica B* **139-140**, 233-236 (1986).

[19] U. Schwarz, A. Grzechnik, K. Syassen, I. Loa, M. Hanfland *Phys Rev Lett* **83**, 4085-4088 (1999).

[20] R.J. Nelmes, M.I. McMahon, J.S. Lovedale, S. Rekhi *Phys Rev Lett* **88**, 155503 (2002).

[21] McMahon MI, Rekhi S, Nelmes RJ (2001) Pressure dependent incommensuration in Rb-IV. *Phys Rev Lett* **87**, 055501:1-4.

[22] M.I. McMahon, R.J. Nelmes *Phys Rev Lett* **93**, 055501 (2004).

[23] P.E. Blöchl *Phys Rev B* **50**, 17953-17979 (1994).

[24] J.P. Perdew, K. Burke, M. Ernzerhof *Phys. Rev. Lett.* **77**, 3865-3868 (1996).

[25] G. Kresse, D. Joubert *Phys Rev B* **59**, 1758-1775 (1999).

[26] The large supercell containing 300 Rb atoms corresponds to a rather small Brillouin zone. This legitimate us to take only a single Γ point in the calculations of the electron density.

[27] I.M. Mryglod, I.P. Omelyan, M.V. Tokarchuk *Mol. Phys.* **84**, 235-259 (1995).

[28] T. Bryk, I. Mryglod, T. Scopigno, G. Ruocco, F.A. Gorelli, M. Santoro *J Chem Phys* **133**, 024502 (2010).

[29] T. Bryk *Eur Phys J Spec Top* **196**, 65-83, (2011).

[30] A.D. Becke, K.E. Edgecombe *J Chem Phys* **92**, 5397-5403 (1990).

[31] F.A. Gorelli, M. Santoro, T. Scopigno, M. Krisch, T. Bryk, G. Ruocco, R. Ballerini *Appl. Phys. Lett.* **94**, 074102 (2009).

[32] K. Tsuji, Y. Katayama, Y. Morimoto, O. Shimomura *J Non-Cryst Sol* **205-207**, 295-298 (1996).

[33] M. Marques, M.I. McMahon, E. Gregoryanz, M. Hanfland, C.L Guillaume, C.J. Pickard, G.J. Ackland, R.J. Nelmes *Phys Rev Lett* **106**, 095502 (2011).

[34] L. Xu, P. Kumar, S.V. Buldyrev, S.-H. Chen, P.H. Poole, F. Sciortino, H.E. Stanley *Proc Natl Acad Sci USA* **102**, 16558-16562 (2005).

[35] M. Yao, K. Okada, T. Aoki, H. Endo *J Non-Cryst Sol* **205-207**, 274-277 (1996).

[36] R. Folk, G. Moser *Phys Rev E* **57**, 683-704 (1998).

[37] R. Folk, G. Moser *Europhys Lett* **41**, 177-182 (1998).

[38] D.L. Bylander, L. Kleinman *Phys Rev B* **45**, 9663 (1992).

[39] F. Demmel, D. Pasqualini, C. Morkel *Phys Rev B* **74**, 184207 (2006).

[40] P.F. McMillan, *J. Mater. Chem.* **14**, 1506 (2004).

[41] E. Rapoport, *J. Chem. Phys.* **46**, 2891 (1967); *J. Chem. Phys.* **48**, 1433 (1968); *Phys. Rev. Lett.* **19**, 345 (1967).

[42] G. Kresse, J. Furthmüller *Comput Mat Sci* **6**, 15-50 (1996).

[43] G. Kresse, J. Furthmüller J *Phys Rev B* **54**, 11169-11186 (1996).